

Flow Test: Particle-Level and Macroscale Analyses

by Hyun-Ki Kim, Douglas D. Cortes, and J. Carlos Santamarina

The physical interpretation of the flow test is investigated by conducting image-monitored flow tests on mortars prepared with mixtures of natural round sand and crushed angular sand to evaluate the progression of flow and the effect of aggregate shape characteristics on cement mortar rheology. The evolution of flow with the number of drops follows a hyperbolic trend. When analyzed within an energy-based framework, it is found that both the base shear at the mortar-plate interface and the internal energy loss in shear deformation are functions of the shear resistance within the mortar. This is further confirmed with mortars prepared with varying quantities of round particles. It is also shown that particle shape affects packing density and the mobilized friction between aggregates; therefore, particle shape defines the amount of paste required to reduce grain interaction to attain adequate flow.

Keywords: aggregate; flow; hydraulic cement; manufactured sand; rheology.

INTRODUCTION

Various tests employ vibration to measure the rheological properties or to evaluate the workability of cement mixtures quantitatively. These include: compaction test (Walz test), Vebe consistometer, Powers remolding test, Thaulow tester, flow table test (DIN flow table), Angels flow box test, LCL flow test, Wigmore consistometer, vibropenetrator, inverted slump cone test, vertical pipe apparatus, vibrating slope apparatus, settlement column segregation test, and vibratory flow meter (Koehler and Fowler 2003).

The flow table test (DIN flow table [DIN 1048 1972; BS EN 12350-5]) and the flow test (ASTM C 1437 2001) are similar: a cone-shaped mold is used to give the initial shape of the specimen, multiple jolts (drops) are applied to spread the specimen, and the horizontal spread of the specimen is measured. Previous studies with the DIN flow table test have shown that (Diamond and Bloomer 1977, Mor and Ravina 1986, Tattersall 1991, Bartos 1992, and Koehler and Fowler 2003):

- The DIN flow table test is simple, inexpensive, and can be readily used in the field.
- Test results are difficult to analyze and are not necessarily adequate to investigate shear rate effects.
- The specimen spread becomes homogenized as the number of jolts increases.
- The initial spread and the final spread after 15 jolts are linearly correlated.
- The spread is nonlinearly related to the number of jolts.
- Specimen slump and spread correlate linearly when the slump is greater than 177.8 mm (7 in.).

In the context of workability assessment tests, the flow test (ASTM C 124 1971) is a quantitative, yet empirical, single-point test (Tattersall and Banfill 1983). It was withdrawn in 1973 because its use in the field was deemed cumbersome compared with the slump test (ASTM C 143; Roy and Idorn [1993])—A detailed analysis of the slump test can be found in Murata [1984] and Schowalter and Christensen [1998].

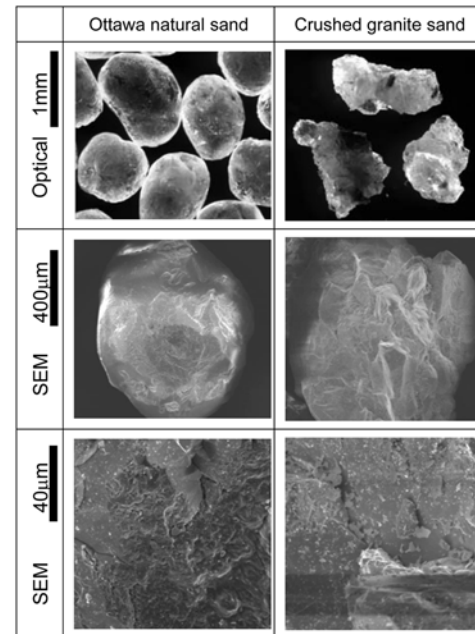


Fig. 1—Microscopic images of natural Ottawa sand and crushed granite sand. (Note: 1 mm = 1000 µm = 0.039 in.)

The flow test was later reinstated in 2001 for its unique advantages, including reproductivity and standardization (ASTM C 1437 2001). Still, the significance of flow test results remains unclear.

RESEARCH SIGNIFICANCE

The purposes of this study are to gain new insight into the underlying physical processes involved in the flow test (ASTM C 1437 2001), to assess its ability to capture fresh mortar rheology, and to address the effects of particle shape on mortar workability. The methodology consists of recording the evolution of flow and developing complementary mathematical analyses.

EXPERIMENTAL INVESTIGATION

Materials

Natural Ottawa sand (OS) and crushed granite sand (CS) of the same particle size D ($0.85 \text{ mm} > D > 0.60 \text{ mm}$ [$0.03 \text{ in.} > D > 0.02 \text{ in.}$]) are selected to prepare mixtures with different mass fractions. OS is round, semi-spherical, and smooth quartzite aggregate, while CS is angular, platy, and rough. Surface characteristics can be inferred from Fig. 1 (optical

ACI Materials Journal, V. 104, No. 3, May-June 2007.

MS No. M-2006-248 received June 14, 2006, and reviewed under Institute publication policies. Copyright © 2007, American Concrete Institute. All rights reserved, including the making of copies unless permission is obtained from the copyright proprietors. Pertinent discussion including authors' closure, if any, will be published in the March-April 2008 *ACI Materials Journal* if the discussion is received by December 1, 2007.

Hyun-Ki Kim is a Postdoctoral Fellow in the School of Civil and Environmental Engineering at the Georgia Institute of Technology, Atlanta, Ga., where he received his PhD. His research interests include multi-scale modeling of granular materials, wave-based nondestructive testing, and the development of engineering solutions for waste and recycled materials.

Douglas D. Cortes is a Graduate Research Assistant in the School of Civil and Environmental Engineering at the Georgia Institute of Technology where he received his BS in civil engineering. His research interests include particle scale phenomena and the effects of particle shape and surface roughness on dry and wet granular flow.

J. Carlos Santamarina is the Goizueta Professor in the School of Civil and Environmental Engineering at the Georgia Institute of Technology. His research interests include particulate materials and phenomena.

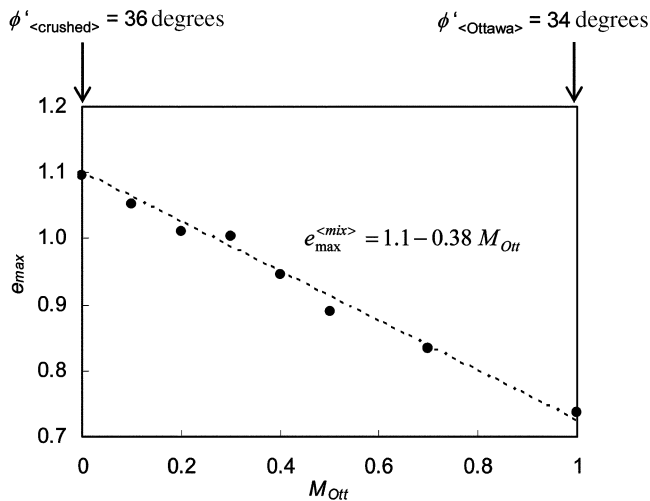


Fig. 2—Maximum void ratio e_{max} versus mass fraction of Ottawa sand M_{Ott} .

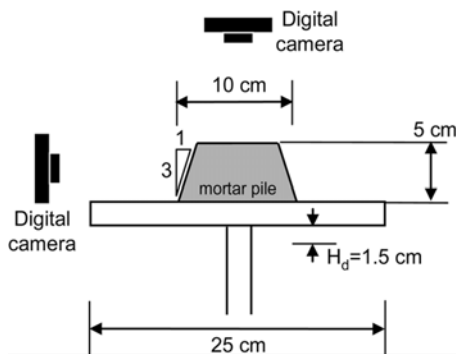


Fig. 3—Schematic diagram of test and devices (H_d is drop height). (Note: 1 cm = 0.39 in.)

stereomicroscope and scanning electron microscope). Clear differences in angularity are observed in the mm-scale. Roughness and indentations on the surface of crushed granite are seen at a scale of approximately 100 μm . However, differences vanish at the 10 μm scale. Therefore, crushing defines shape and contributes to surface roughness at a scale of approximately 10% of the particle diameter.

Mixtures are prepared with different mass fractions of OS: 0% (this is the pure CS), 10, 20, 30, 40, 50, 70, and 100% (this is the pure OS). Gravimetric mixing ratios are kept constant; in particular, the fine aggregate-to-cement ratio (FA/C) is 2.0, and the water-to-cement ratio (w/c) is 0.46 in all cases. Mixing is implemented in a standard laboratory mixer. Angular CS produces mixtures with lower workability than spherical OS for a given water and paste content (Quiroga and Fowler 2003).

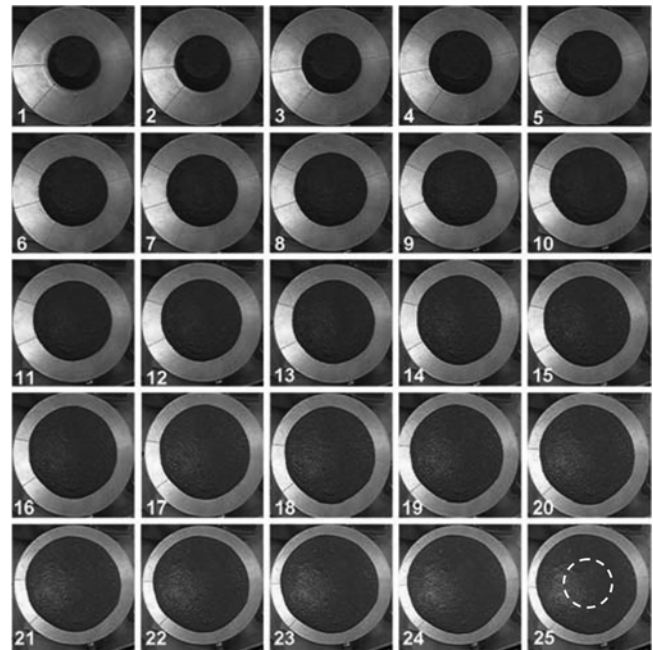


Fig. 4—Photographs of gradual mortar spread (100% natural Ottawa sand mortar). Drop number i is shown in white. The dotted circle shown in picture after 25th drop indicates initial imprint of mortar pile.

The maximum void ratio e_{max} is measured for all sand mixtures following ASTM D 4254 (2000). Figure 2 shows that the CS packs in a looser state ($e_{max} = 1.1$) than the OS ($e_{max} = 0.74$). The maximum void ratio for all mixtures can be estimated in terms of mass fraction of OS M_{Ott} as follows: $e_{max}^{<mix>} = 1.1 - 0.38M_{Ott}$. Despite the higher maximum void ratio, the angular CS exhibits a higher angle of repose or critical state friction angle ($\phi' = 36$ degrees) than the round OS ($\phi' = 34$ degrees) because of enhanced interlocking between angular particles.

Test procedure

The flow test is performed following ASTM C 1437 (2001). Freshly mixed hydraulic cement mortar is placed inside the cone-shaped mold in two layers. Then the mold is removed and the vibrating table is dropped 25 times in 15 seconds. Flow F is defined as $F = (R_{25} - R_0)/R_0 \times 100[\%]$, where R_{25} is the radius of the mortar pile after the 25th drop and R_0 is the initial radius of the mortar pile (ASTM C 1437 2001). In this study, the incremental spread of the mortar pile is recorded using digital photography after each drop, therefore $F_i = (R_i - R_0)/R_0 \times 100[\%]$, where i is the drop number (refer to Fig. 3). Figure 4 shows the evolution of the pile during the first 25 drops for the 100% OS mortar.

Segregation

Segregation can occur between cement paste and aggregates (refer to DIN flow table [Bartos 1992]). The development of segregation is explored in this study using a mixture of 50% natural OS and 50% CS. After 25 drops, the pile is divided into eight sectors, and the sand content in each sector is determined by washing away the paste. Results show that vibrations in the flow test cause no clearly detectable segregation between paste and fine aggregates.

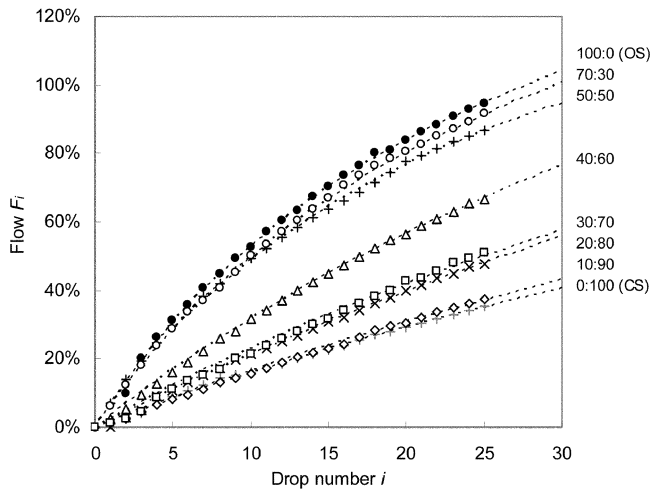


Fig. 5—Flow versus drop number—hyperbolic model predictions. Points are measured data. Lines show fitted hyperbolic model. Numbers indicate mass ratio between Ottawa sand, and crushed granite sand.

EXPERIMENTAL RESULTS AND ANALYSIS

The measured horizontal spread in terms of flow at each i -th drop F_i for all mortars is shown in Fig. 5. There are two salient observations. First, flowability increases as the mass fraction of OS increases. OS begins exerting a strong effect on flow when the mass fraction of OS is $M_{Ott} \geq 0.3$; therefore, the presence of OS is more effective in promoting flow than the CS in hindering it. Mixtures can be classified into round-like, crushed-like, and transitional mixtures. The transition range in this study is observed between $M_{Ott} = 0.3$ and 0.5 .

Second, there is a nonlinear relationship between the mortar spread F_i and the drop number i . As the height of the mortar pile decreases with increasing spread, the driver for spreading decreases while the resistance to flow at the mortar-surface interface increases. Hence, the incremental spread decreases with the number of drops. This suggests a nonlinear hyperbolic trend between flow, $F_i = (R_i - R_0)/R_0$, and drop number i

$$F_i = \frac{i}{a \cdot i + b} \quad (1)$$

The two independent parameters a and b can be replaced by the flow value A at 25 drops and the initial flow rate B at the beginning of the test

$$A = F_{i=25} = \frac{25}{25a + b} \quad (2)$$

$$B = \left[\frac{dF}{di} \right]_{i=0} = \left[\frac{b}{(ai + b)^2} \right]_{i=0} = \frac{1}{b} \quad (3)$$

Either set of model parameters, (A, B) or (a, b) , can be extracted from the data by fitting the hyperbolic model using least squares. The L_2 norm is

$$L_2 = \left[\sum_i |F_i^{(measured)} - F_i^{(estimated)}|^2 \right]^{1/2} \quad (4)$$

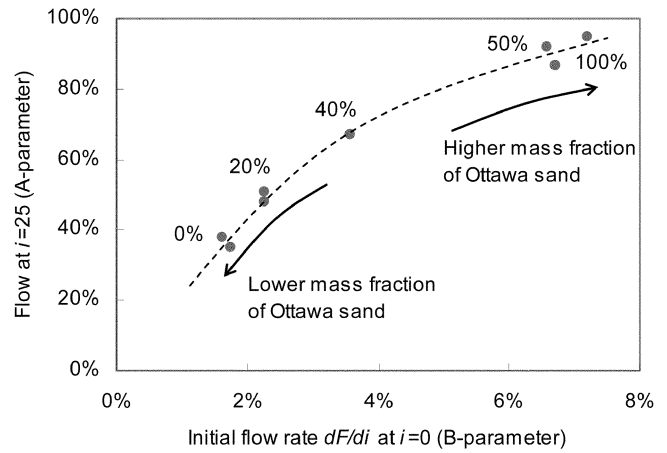


Fig. 6—Flow at 25 drops (A-parameter) versus initial flow rate (B-parameter).

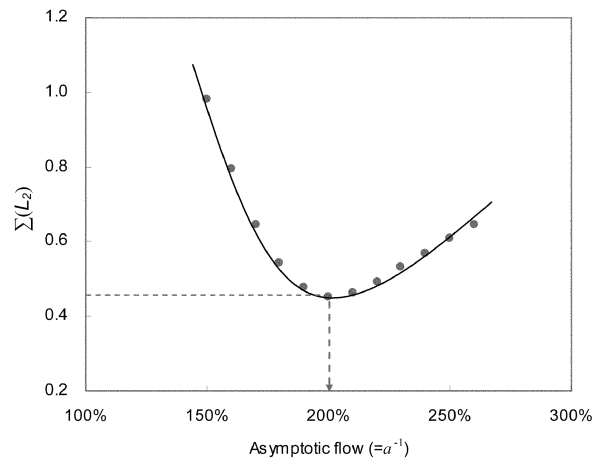


Fig. 7—Identification of common asymptotic flow value, $F_{i \rightarrow \infty} = a^{-1}$, for all mixtures. Total L_2 error is minimized when the asymptotic flow is, $F_{i \rightarrow \infty} \approx 200\%$.

Fitted lines are shown together with the measured data in Fig. 5. Both the A parameter (flow at 25 drops) and the B parameter (initial flow rate) increase with the mass fraction of OS. Furthermore, there is a positive correlation between A and B , as shown in Fig. 6.

The A - B correlation suggests the possibility of a single-parameter hyperbolic model. Furthermore, note that the height of mortar piles converges towards a low asymptotic value as the drop number increases. The associated flow value is extracted from a formal inversion analysis based on the L_2 norm. The computed value is $F_{i \rightarrow \infty} = a^{-1} \approx 200\%$ (Fig. 7). Then, the hyperbolic model can be written as a function of a single parameter, the initial flow rate $B = 1/b$, and Eq. (1) becomes

$$F_i = \frac{i}{0.5i + b} \quad (5)$$

When this equation is fitted to the data, the trends are indistinguishable from those shown in Fig. 5.

ANALYTICAL INVESTIGATION

As the number of drops increases, the height of the pile decreases; therefore, the potential energy E_p decreases as well. The potential energy lost at the i -th drop (E_p) _{i} is spent in deforming the mortar pile E_{deform} and spreading it against

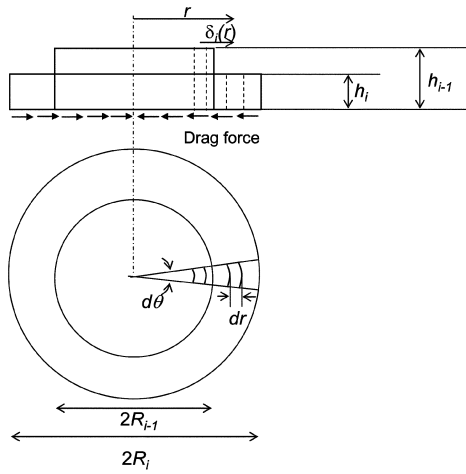


Fig. 8—Schematic diagram of mortar pile flow between two consecutive drops $i - 1$ and i .

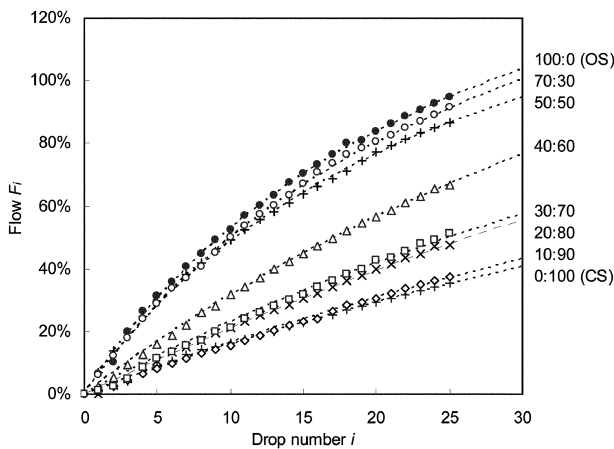


Fig. 9—Flow versus drop number—energy-based model predictions. Points are measured data. Lines show fitted energy model. Numbers indicate mass ratio between Ottawa sand and crushed granite sand.

the interfacial shear at the base $E_{base\ shear}$. The energy balance for the i -th drop is

$$(E_p)_i = (E_{deform})_i + (E_{base\ shear})_i \quad (6)$$

It is assumed herein that: 1) wet mixtures preserve volume; 2) the energy spent in deforming the mortar pile E_{deform} is linearly proportional to the incremental global deviatoric strain; and 3) the interfacial shear energy $E_{base\ shear}$ between a unit area of the deformed mortar pile and the flow table surface is linearly proportional to the incremental radial spread (refer to Fig. 8). Then, each energy component becomes

$$(E_p)_i = w \left(h_d + \frac{h_{i-1} - h_i}{2} \right) = V_0 \gamma_t \left[h_d + \frac{V_0}{2\pi} \left(\frac{1}{R_{i-1}^2} - \frac{1}{R_i^2} \right) \right] \quad (7)$$

$$(E_{deform})_i = \int_{V_0} \tau_0 \cdot \frac{2}{3} (\varepsilon_h - \varepsilon_r)_i dV = \tau_0 \cdot \left(\frac{R_i^2 - R_{i-1}^2}{R_i^2} \right) V_0 \quad (8)$$

$$\text{(for } \varepsilon_{vol} = 0, \varepsilon_r = -0.5\varepsilon_h \text{)}$$

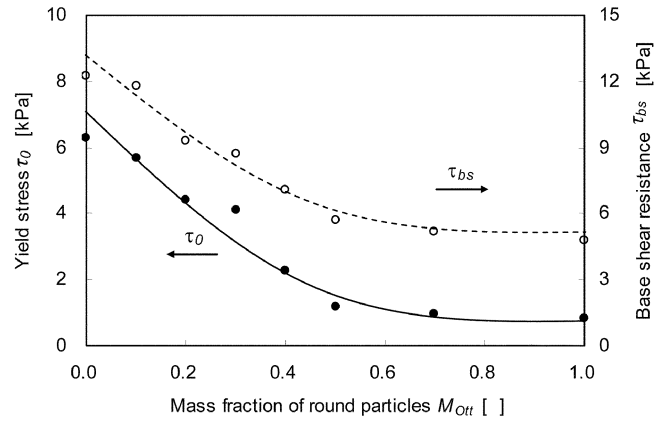


Fig. 10—Energy-based model—fitted model parameters τ_0 and τ_{bs} . (Note: 1 kPa = 0.145 psi.)

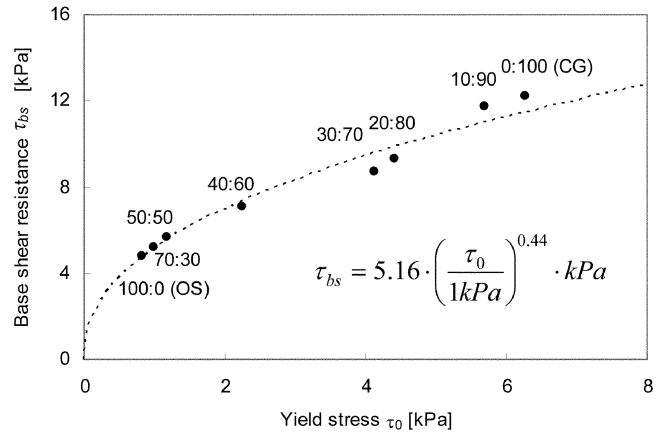


Fig. 11—Correlation between yield stress τ_0 and base shear resistance τ_{bs} . (Note: 1 kPa = 0.145 psi.)

$$\begin{aligned} (E_{base\ shear})_i &= \int_{A_i} \tau_{bs} \delta_i(r) dA \\ &= \tau_{bs} \int_0^{R_i} \int_0^{2\pi} \left[\left(\frac{R_i}{R_{i-1}} - 1 \right) \cdot r \right] \cdot r \cdot d\theta dr \\ &= \frac{2}{3} \pi \cdot \tau_{bs} \cdot \left(\frac{R_i}{R_{i-1}} - 1 \right) \cdot R_i^3 \end{aligned} \quad (9)$$

where w is the weight of the cement mortar pile, h_d is the drop height of the flow table, h_i and R_i are the height and radius of the mortar pile after the i -th drop, γ_t is the unit weight of the mortar, V_0 is the volume of the mortar pile, τ_0 is the shear resistance of the mortar, τ_{bs} is the base shear resistance between the mortar pile and the flow table, and $\delta_i(r)$ is the incremental spread of the mortar pile at a radial distance r during the i -th drop. The implicit solution of the mortar spread R_i in terms of parameters τ_0 and τ_{bs} is obtained by substituting Eq. (7) through (9) into Eq. (6)

$$\begin{aligned} &V_0 \gamma_t \left\{ h_d + \frac{V_0}{2\pi} \left(\frac{1}{R_{i-1}^2} - \frac{1}{R_i^2} \right) \right\} \\ &= \tau_0 \cdot \left(\frac{R_i^2 - R_{i-1}^2}{R_i^2} \right) \cdot V_0 + \frac{2}{3} \pi \cdot \tau_{bs} \cdot \left(\frac{R_i}{R_{i-1}} - 1 \right) \cdot R_i^3 \end{aligned} \quad (10)$$

Figure 9 shows the flow-versus-drop trends of all mixtures and the fitted energy model. The fitted model parameters in each case, τ_0 and τ_{bs} , are plotted versus the mass fraction of round particles (that is, OS) in Fig. 10. The two parameters are affected by the mass fraction of round particles M_{Oit} as discussed previously: the presence of round particles decreases the resistance to flow when $M_{Oit} < 0.5$ and determines flow when $M_{Oit} > 0.5$. The apparent correlation between τ_0 and τ_{bs} observed in Fig. 10 is confirmed in Fig. 11. The fitted trend is

$$\tau_{bs} = 5.16 \cdot \left(\frac{\tau_0}{1 \text{ kPa}} \right)^{0.44} \text{ [kPa]} \quad (11)$$

Once again, a single controlling parameter becomes apparent; in this case it is the mortar shear resistance τ_0 .

The flowability of mortar is controlled by its shear resistance at the given shear rate. Data presented herein show that shear resistance is in part due to frictional losses at particle contacts. Viscous losses may be involved as well; however, the relative contributions cannot be inferred from flow test data alone. It has been shown that the interaction between cement paste and aggregates governs the rate-dependent viscous dissipation (Larrard 1999; Tattersall and Banfill 1983): the presence of rigid particles produces higher shear rate within the cement paste, and increases the viscous dissipation. From this perspective, angular sands have higher specific surface and promote greater interfacial resistance.

On the other hand, angular particles yield a looser packing density (that is, higher e_{max}) and higher frictional resistance (Fig. 2). Both packing and frictional effects lead to lower flow for the same volume ratio of $V_{aggregate}$ to V_{paste} as particle angularity increases (Fig. 5). This contributes to the strong effect of particle shape on the rheology of mortar (Tattersall 1991). Conversely, more paste is required to keep angular particles apart to decrease their interaction and increase flow.

CONCLUSIONS

The detailed experimental and analytical study of the flow test permits extracting the following conclusions:

- There is a nonlinear relationship between flow F_i and drop number i . A single parameter hyperbolic equation adequately fits measured data;
- An energy-based physical model explains the relative contribution of internal energy loss in shear and base shear along the mortar-surface interface. The two model parameters, mortar shear resistance τ_0 , and mortar-to-base shear resistance τ_{bs} , are correlated suggesting internal shear as a single loss mechanism;

- Flow reflects the packing characteristics and the frictional resistance of the fine aggregate. Both are affected by particle shape. In particular, crushed angular aggregates yield loose packing density and high friction. Hence, more paste is required to keep angular particles apart and to attain adequate flow;
- The presence of round particles controls flow when the mass fraction of round particles exceeds 30 to 50%.

ACKNOWLEDGMENTS

This research is supported by a grant from the Georgia Department of Transportation and Georgia Crushed Stone Association. Additional support was provided by the Goizueta Foundation.

REFERENCES

- ASTM C 124-71, 1971, "Method of Test for Flow of Portland-Cement Concrete by Use of the Flow Table," ASTM International, West Conshohocken, Pa. (withdrawn 1973)
- ASTM C 143-05, 2005, "Standard Test Method for Slump of Hydraulic Cement Concrete," ASTM International, West Conshohocken, Pa., 4 pp.
- ASTM C 1437-01, 2001, "Standard Test Method for Flow of Hydraulic Cement Mortar," ASTM International, West Conshohocken, Pa., 2 pp.
- ASTM D 4254-00, 2000, "Standard Test Methods for Minimum Index Density and Unit Weight of Soils and Calculation of Relative Density," ASTM International, West Conshohocken, Pa., 9 pp.
- Bartos, P., 1992, *Fresh Concrete: Properties and Tests*, Elsevier, 292 pp.
- BS EN 12350-5, 2000, "Testing Fresh Concrete: Flow Table Test," British-Adopted European Standard, London, UK, 8 pp.
- De Larrard, F., 1999, *Concrete Mixture Proportioning, A Scientific Approach*, E&FN Spon, London, 421 pp.
- Diamond, C. R., and Bloomer, S. J., 1977, "A Consideration of the DIN Flow Table," *Concrete*, V. 11, No. 12, pp. 29-30.
- DIN 1048, 1972, "Testing Methods of Concrete," *Deutsches Institut für Normung*, No. V, Clause 312, Berlin, Germany.
- Koehler, E. P., and Fowler, D. W., 2003, "Summary of Concrete Workability Test Methods," *ICAR Report 105-1*, International Center for Aggregates Research, the University of Texas at Austin, Austin, Tex., 83 pp.
- Mor, A., and Ravina, D., 1986, "The DIN Flow Table: A Complement to the Slump Test for High Slump Concrete," *Concrete International*, V. 8, No. 12, Dec., pp. 53-56.
- Murata, J., 1984, "Flow and Deformation of Fresh Concrete," *Materials and Structures*, V. 17, No. 2, pp. 117-129.
- Quiroga, P., and Fowler, D., 2003, "The Effects of Aggregates Characteristics on the Performance of Portland Cement Concrete," *ICAR Report 104-1F*, International Center for Aggregates Research, the University of Texas at Austin, Austin, Tex., 358 pp.
- Roy, D. M., and Idorn, G. M., 1993, "Concrete Microstructure," *Strategic Highway Research Program Report SHPR-C-340*, National Academy of Sciences, 179 pp.
- Schwalter, W. R., and Christensen, G., 1998, "Toward a Rationalization of the Slump Test for Fresh Concrete: Comparisons of Calculations and Experiments," *Journal of Rheology*, V. 42, No. 4, pp. 865-870.
- Tattersall, G. H., 1991, *Workability and Quality Control of Concrete*, E&FN Spon, London, UK, 269 pp.
- Tattersall, G. H., and Banfill, P. F. G., 1983, *The Rheology of Fresh Concrete*, Pitman Advanced Publishing Program, 356 pp.

Reproduced with permission of the copyright owner. Further reproduction prohibited without permission.